Free Radicals in L-Arginine·HCl·H_2O Single Crystals X-irradiated at 66K- EPR, ENDOR, EIE and DFT Studies

Yiying Zhou and William H. Nelson*

Department of Physics and Astronomy, Georgia State University, P.O. Box 4106, Atlanta, Georgia 30302-4106

Received: December 17, 2009; Revised Manuscript Received: February 23, 2010

X-irradiation of L-arginine hydrochloride monohydrate crystals at 66 K led to at least five radicals detectable with K-band Electron Paramagnetic Resonance (EPR), Electron−Nuclear DOuble Resonance (ENDOR) and ENDOR-induced EPR (EIE) techniques. Radicals R1a and R1b were identified as carboxyl-centered radicals from one-electron reduction, $(H_2OO\dot{C})CH\ (NH_3)^+(CH_2)_3NHC(NH_2)_2^+$ in two different conformations arising from the two geometrically distinct molecules of the asymmetric unit in the crystal. Density-Functional Theory (DFT) calculations on cluster models constructed separately for each molecule of the asymmetric unit support the assignments. Radical R2 was identified as the decarboxylation radical, $\dot{C}H(NH_3)^+(CH_2)_3NHC\ (NH_2)_2^+$. Radical R3, with two proton couplings and one nitrogen coupling, was identified as a radical with the unpaired electron localized on the guanidyl group, $^-(OOC)CH(NH_3)^+(CH_2)_3NH\dot{C}(NH_2)_2^+$. R3 is a product of one-electron reduction different from radicals R1a and R1b. DFT calculations on a cluster model reproduced the experimental values very well and thus supported the assignment of R3. Geometry optimization indicated that the guanidyl group transformed from planar to pyramidal upon trapping the electron. Radical R4 was identified as a side chain dehydrogenation radical, $^-(OOC)CH(NH_3)^+(CH_2)_2\dot{C}H\ NHC(NH_2)_2^+$. It was not possible to collect sufficient data to identify radical R5, although it clearly exhibited hyperfine coupling to one nonexchangeable β-proton.

1. Introduction

Arginine (Chart 1) shares with lysine the distinction of being the amino acid most often in contact with DNA as it interacts with proteins. Together, these two account for more than 20% of the amino acids in the nuclear histones.[1] Crystallographic study of the nucleosome core found that direct interactions between the histones and DNA predominantly involve arginine and lysine, a result indicating their importance in that setting.[2] As well, proteins interact with DNA during various genetic processes. In this more general context, a survey of 129 crystallized protein−DNA complexes revealed a very high incidence of hydrogen bonding interactions between DNA and arginine or lysine. In fact, the analysis indicated a systematic nature to the hydrogen bonding between arginine and guanine, thereby suggesting that the apparent specificity of their interaction is an element of base recognition processes.[3]

Because DNA interacts so closely with proteins in chromatin, several previous studies have focused on the role this association might play in the progression, or inhibition, of chemical damage to DNA initiated by ionizing radiation.[4,5] The basic outcomes are that the histones appear to have a protective effect toward hydroxyl attack but a sensitizing effect toward radical formation. In particular, EPR study of chromatin found an increased yield of DNA-centered radicals from one-electron reduction in comparison to DNA alone, an indication that ionization-produced electrons transferred from the histones to DNA while the oxidation centers (or holes) remained with the histones.[5] Taken together, these results underscore the fact that DNA−protein interactions have an important influence on the processes leading to radiation damage of DNA in vivo.

CHART 1: Zwitterionic and Protonated Arginine As Present in Larginine·HCl·H_2O Single Crystals

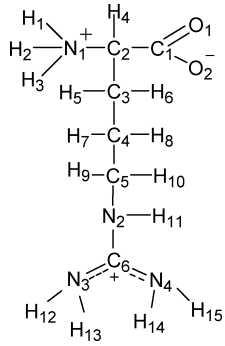

That arginine is an amino acid frequently interacting with DNA introduces the question of what role it might play in the way proteins influence ionization-initiated DNA damage. As a step toward addressing this question, and following our recent report on L-lysine hydrochloride dihydrate,[6] we chose to investigate radical formation in L-arginine·HCl·H_2O (L-arg·HCl·H_2O) single crystals X-irradiated (and detected) at 66 K by means of EPR/ENDOR spectroscopy supplemented with DFT-based calculations. There are very few previous studies of irradiated arginine in condensed media. In an examination of radical decay kinetics in crystalline amino acids under controlled warming from room to higher temperatures, Joshi and Johnsen included L-arg·HCl·H_2O and proposed that the radical present in major concentration was the molecule dehydrogenated at C5 (see Chart 2), although they did not characterize it.[7] Using EPR techniques, Aydin et al. also reported evidence for the C5 dehydrogenation radical in L-arginine powder γ-irradiated at room temperature.[8] More recently, Olsen studied L-arginine phosphate monohydrate (LAP) single crystals

* To whom correspondence should be addressed. Tel.: +1 4044135104. Fax: +1 4044135117. E-mail: wnelson@gsu.edu.

10.1021/jp911943n
Published on Web 04/05/2010

CHART 2: Radical from Dehydrogenation at C5

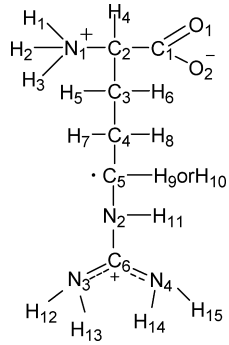

CHART 3: Carboxyl-Centered Radical from One-Electron Reduction

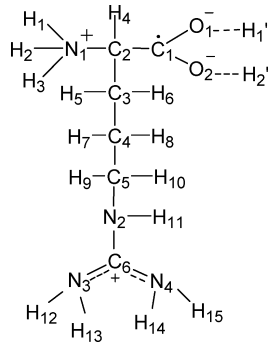

CHART 4: Decarboxylation Radical

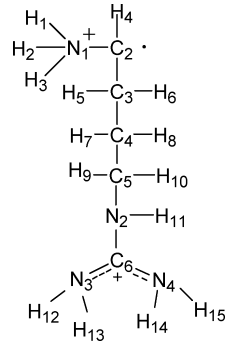

using EPR/ENDOR techniques supplemented with DFT calculations.[9] Results from irradiation and study of LAP at 77 K showed a significant concentration of the radical from electron trapping at the carboxyl (see Chart 3), from decarboxylation (see Chart 4), and from dehydrogenation at C5. Products identified following irradiation and study of LAP at room temperature were the main-chain deamination radical (see Chart 5) and the C5 dehydrogenation radical (see Chart 2).

The work reported here found that X-irradiation of L-arg·HCl·H_2O single crystals at 66 K led to significant concentrations of the radicals from electron capture by the carboxyl, from decarboxylation, and from dehydrogenation at C5. In addition, the results indicate a significant concentration of the radical from electron capture by the guanidyl group on the arginine side chain. (Results from warming the crystals to room temperature, and from irradiating them at room temperature, are complex and will be described elsewhere.)

The guanidyl-centered radical is significant for two reasons. One is that this portion of arginine, located at the end of its side chain, is the part most commonly in contact with DNA as it interacts with proteins. The second reason comes from interest

CHART 5: Main-Chain Deamination Radical

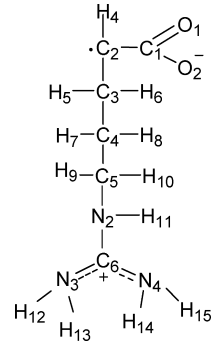

in arginine by the mass spectrometry community with a focus on its behavior following electron capture. Specifically, in a series of experimental and computational studies aimed at describing electron capture dissociation (ECD), arginine became a useful subject because of the amide groups on both the main and side chains.[10] In the usual mass spectrometric procedures, the molecules are protonated, sometimes multiply; in the case of arginine, a favored protonation site is the guanidyl group of the side chain and that group is protonated in L-arginine·HCl·H_2O. As a result, except that arginine is zwitterionic in the crystal, the guanidyl-centered electron adduct observed here is a condensed-media correlate of that formed initially by electron capture in the gas phase within a mass spectrometer.

2. Experimental and Computational Methods

L-arg·HCl·H_2O single crystals were grown from saturated aqueous solutions of the material (Sigma Chemical Co.) by slow evaporation at room temperature. Partially deuterated crystals were prepared similarly from solutions of material, previously recrystallized at least three times from deuterium oxide, placed in a desiccator at room temperature. Dow and Jensen[11] reported that the crystal structure is monoclinic ($P2_1$), with two molecules in the asymmetric unit, denoted as molecules A and B, and with four molecules (two each from molecules A and B) per unit cell.

In the crystals, the arginine molecule is a zwitterionic cation with positive charges on both the main chain amino group and the side chain guanidyl group, and with a single negative charge on the main chain carboxyl group. (See Chart 1) The geometries of molecules A and B are similar except for their carboxyl group: the O1O2C2C1 groups (see Chart 1) of molecules A and B are planar with similar torsion angles $\angle$O1−O2−C2−C1 $< \sim 2°$, H4 in molecule A is $\sim 20°$ farther from the carboxyl plane than that in molecule B. Guanidyl groups in both molecules A and B are planar.

In L-arg·HCl·H_2O arginine participates in an extensive system of hydrogen bonds. The two carboxyl oxygen atoms and all the N−H hydrogen atoms in molecules A and B are involved in hydrogen bonds to atoms in neighboring molecules, and there are no intramolecular hydrogen bonds. The hydrogen bonds to the main-chain amino and side-chain guanidyl protons are similar for molecules A and B. However, the arrangements are different for hydrogen bonds to the carboxyl oxygen atoms. These differences in the arrangement of hydrogen bonds to the carboxyl groups, and the differences in the carboxyl groups' geometries for molecules A and B, apparently led to the two different conformations of radical R1 as described below.

Both normal and deuterated crystals were X-irradiated at 66 K (pumped liquid nitrogen) for about 3 h to a dose of 100−200

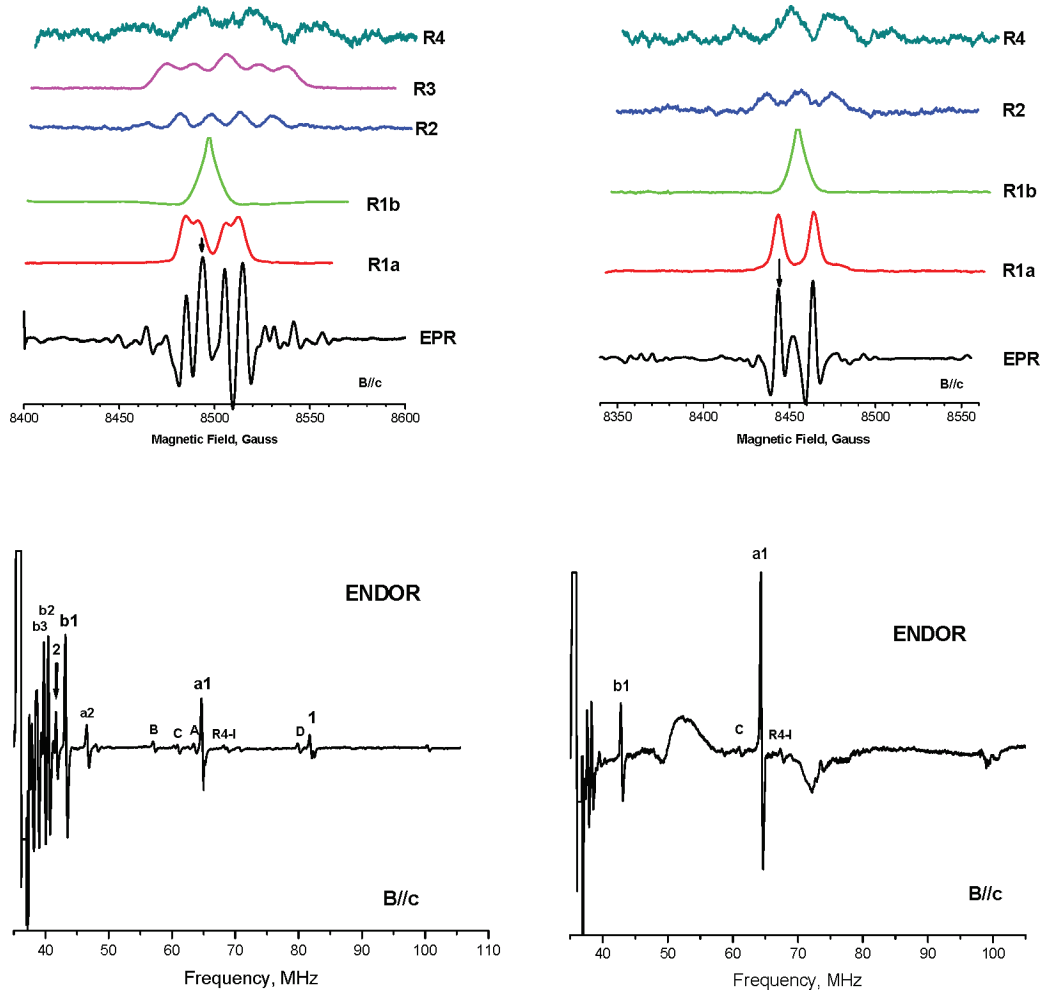

Figure 1. EIE patterns and second-derivative EPR and first-derivative ENDOR spectra detected immediately after the X-irradiation at 66 K for the normal (left) and the partially deuterated (right) L-arg·HCl·H_2O crystals with the magnetic field along *c*. The arrows in the EPR indicate the magnetic field chosen for the ENDOR spectra in the lower panels.

kGy. Subsequently, the K-band EPR, ENDOR, and EIE were recorded at 66 K. The methods of crystal orientation, temperature control and monitoring, data analysis, and spectrum simulations were reported previously.[12] The WINSIM[13] program was used extensively for spectrum simulations to test the validity of proposed radical structures. WINSIM creates a first-order simulated EPR spectrum and provides automatic adjustment of the coupling parameters to create the best fit to an experimental pattern. In this work, crystallographic *a*, *b*, and *c** directions were chosen as the orthogonal reference system. The *g*-tensors for all the radicals are virtually isotropic and near the free electron value, 2.0023.

The DFT computations were performed using the Gaussian03 suite of programs[14] to help with identifying the radicals and to investigate their reorientations. All initial atomic coordinates were taken from the crystallographic studies.[11] These initial radical geometries were optimized with DFT methods using the B3LYP functional in combination with the 6-31G(d,p) basis set. Single-point calculations for hyperfine coupling constants of the radicals were performed with DFT using the higher basis set 6-311G(2d,f).[15] The keyword "NOSYMM" was used for all calculations to prevent the Cartesian coordinates of the radical model from rotating or shifting with respect to the reference frame. This approach allows the eigenvectors of the calculated tensors to be compared directly with those obtained from the experiments.[16] In this work, the cluster models were constructed as described below. The final models chosen for the radicals were those giving computational results with (1) no single coupling values >15 MHz and (2) no single eigenvector >25° from experimental values.[16] (For β-couplings, only the eigenvectors associated with the eigenvalues associated with the maximum coupling were compared.)[17] To finalize the assignment by demonstrating that the radical form could provide the observed hyperfine couplings, it sometimes was necessary to manually adjust the atomic coordinates as described in the discussion below. The rationale for this is that structural rearrangements in crystals upon radical formation can be hindered by intermolecular interactions, and it is difficult to fully account for these intermolecular interactions in the systems used for geometry optimizations. Both α- and β- hyperfine couplings have known dependencies on radical geometry. Thus, our objective with the manual adjustments was to verify the existence of radical structures, chemical and geometrical, yielding computed hyperfine couplings compatible with those measured.

3. Results and Analysis

Figure 1 shows EPR spectra recorded from normal and partially deuterated L-arg·HCl·H_2O single crystals immediately after X-irradiation at 66 K with the magnetic field along *c*. EPR for the normal crystal is dominated by a four-line hyperfine pattern in the center with some weak lines on both sides; EPR from the partially deuterated crystal is dominated by a two-line pattern at the center, with weak lines on both sides that are quite different from those of the normal crystal. The spectral differences indicate that at least

TABLE 1: Hyperfine Coupling Tensors a1−a3 for Radical R1a and Tensor b1 for R1b, Compared to Crystallographic Directions Related to the Carboxyl-Centered Radical from Molecules A and B[a,b]

tensors	principal values[a,b]	isotropic values[a]	anisotropic values[a]	eigenvectors[b] *a*	*b*	*c**
a1	60.28(2)	52.92	7.36	0.093(1)	0.527(3)	−0.845(2)
	50.69(2)		−2.23	0.575(1)	−0.721(2)	−0.387(3)
	47.80(2)		−5.12	0.813(1)	0.450(2)	0.370(2)
a2	23.62(3)	9.30	14.32	0.198(1)	−0.320(7)	−0.927(5)
	3.03(3)		−6.27	0.599(1)	−0.709(6)	0.372(6)
	1.24(4)		−8.06	0.776(0)	0.629(1)	−0.051(4)
a3	16.90(5)	1.69	15.21	0.874(1)	−0.483(5)	−0.058(8)
	−3.71(10)		−5.40	0.426(2)	0.817(6)	−0.388(17)
	−8.11(11)		−9.80	0.235(4)	0.314(18)	0.920(8)
b1	21.66(2)	10.60	11.06	0.416(1)	0.531(2)	−0.738(10)
	6.10(2)		−4.50	0.897(1)	−0.375(9)	0.235(4)
	4.04(2)		−6.56	0.152(1)	0.760(7)	0.632(3)

crystallographic directions[c]	eigenvectors[b] *a*	*b*	*c**
H4...C1(MA)	0.202	0.466	−0.862
H1′...C1(MA)	0.138	−0.546	−0.826
H2′...C1(MA)	0.998	−0.049	−0.028
H3′...C1(MA)	0.672	−0.504	−0.543
H4′...C1(MA)	−0.433	−0.868	−0.244
H4...C1(MB)	0.268	0.464	−0.844

		angle diff (deg)[e]
eigenvector* of coupling a1[d]	H4...C1(MA)	6.9
eigenvector* of coupling a2[d]	H1′...C1(MA)	14.6
eigenvector* of coupling a3[d]	H2′...C1(MA)	26.2
eigenvector* of coupling b1[d]	H4...C1(MB)	11.3

[a] Values in MHz. [b] Numbers in parentheses are the estimated uncertainties in the respective values as reported by the statistical analysis. [c] H1′−H4′ are protons in the neighboring molecules and involve hydrogen bonds to the carboxyl group of molecule A, as denoted in Figure 2. "MA" and "MB" stand for molecules A and B, respectively. [d] The eigenvector* is that associated with the maximum eigenvalue. [e] "Angle diff (deg)" is the angular difference between the experimental eigenvector* and the crystallographic directions in degrees.

one coupling contributing to the four-line pattern comes from an exchangeable proton, and that some couplings of the weak lines also are due to exchangeable protons.

The four-line hyperfine pattern is resolved in the normal crystal's EPR only when the magnetic field is near *c*. With the field along *a* (B//*a*) and *b* (B//*b*), the EPR is a wide two-line pattern with slight shoulders; EPR from the normal and partially deuterated crystals at these orientations are nearly the same. These characteristics indicate that the coupling in the center pattern that becomes unresolvable in the EPR at *a* and *b* is from an exchangeable proton, and that the other coupling is from a nonexchangeable proton.

ENDOR spectra for B//*c* from the two crystal types, with the magnetic field locked to the center EPR peaks, also are shown in Figure 1. At least five distinct EIE patterns were detected for the normal crystal with B//*c*, as is shown in the upper left panel of Figure 1. These distinct patterns allowed us to assign the respective ENDOR lines to four distinct radicals: R1a and R1b, R2, R3, and R4. (R1a and R1b turn out to be the same radical type in different conformations.) Comparison of the normal-crystal EPR and EIE patterns for B//*c*, as shown in Figure 1 (upper left panel), indicates that the central four-line pattern is mainly from radical R1a, and that some weak lines on both sides are from radicals R2-R4; EPR from R1b overlaps one of the central four peaks at this orientation. One additional distinct EIE pattern was detected from the normal crystal for B//*a* (see Figure S12 of the Supporting Information) and was assigned to an additional radical, R5.

3.1. Radical R1a: Carboxyl-Centered One-Electron Reduction Radical from Molecule A. For the normal crystal, ENDOR lines a1 and a2 (Figure 1, lower left) gave the dominant four-line pattern in the center of the EPR for B//*c* and were assigned to radical R1a; one additional ENDOR line, labeled a3, was detected at B//*a* for R1a, and this coupling was difficult to detect at B//*c* because it almost overlaps with the free proton line. Couplings a1 and a2 were sufficient to simulate the dominant four-line hyperfine pattern in the EPR spectrum for B near *c*; at orientations farther from *c*, coupling a2 became small enough that only a1 was resolvable in the EPR. The result was a strong two-line pattern at the center. Coupling a3 always was very small and was unresolvable in the EPR at all orientations.

From comparison of the ENDOR spectra for the normal and partially deuterated crystals, as shown in Figure 1 for B//*c*, coupling a1 is from a nonexchangeable hydrogen, while couplings a2 and a3 are from exchangeable ones. Moreover, the four-line EIE pattern of R1a for B//*c* (Figure 1 lower left) becomes a two-line EIE pattern as a result of the partial deuteration (Figure 1 lower right). Coupling a1 alone can reproduce the EIE pattern for B//*c* from the partially deuterated crystal. These results confirm that the larger coupling a1 is from a nonexchangeable hydrogen while the smaller coupling a2 is from an exchangeable hydrogen.

Analysis of the ENDOR data gave the hyperfine coupling tensors for a1−a3 as listed in Table 1. Tensor a1 must be from a C−H β-proton because it exhibits moderate anisotropy and axial symmetry and is from a nonexchangeable proton. Tensors

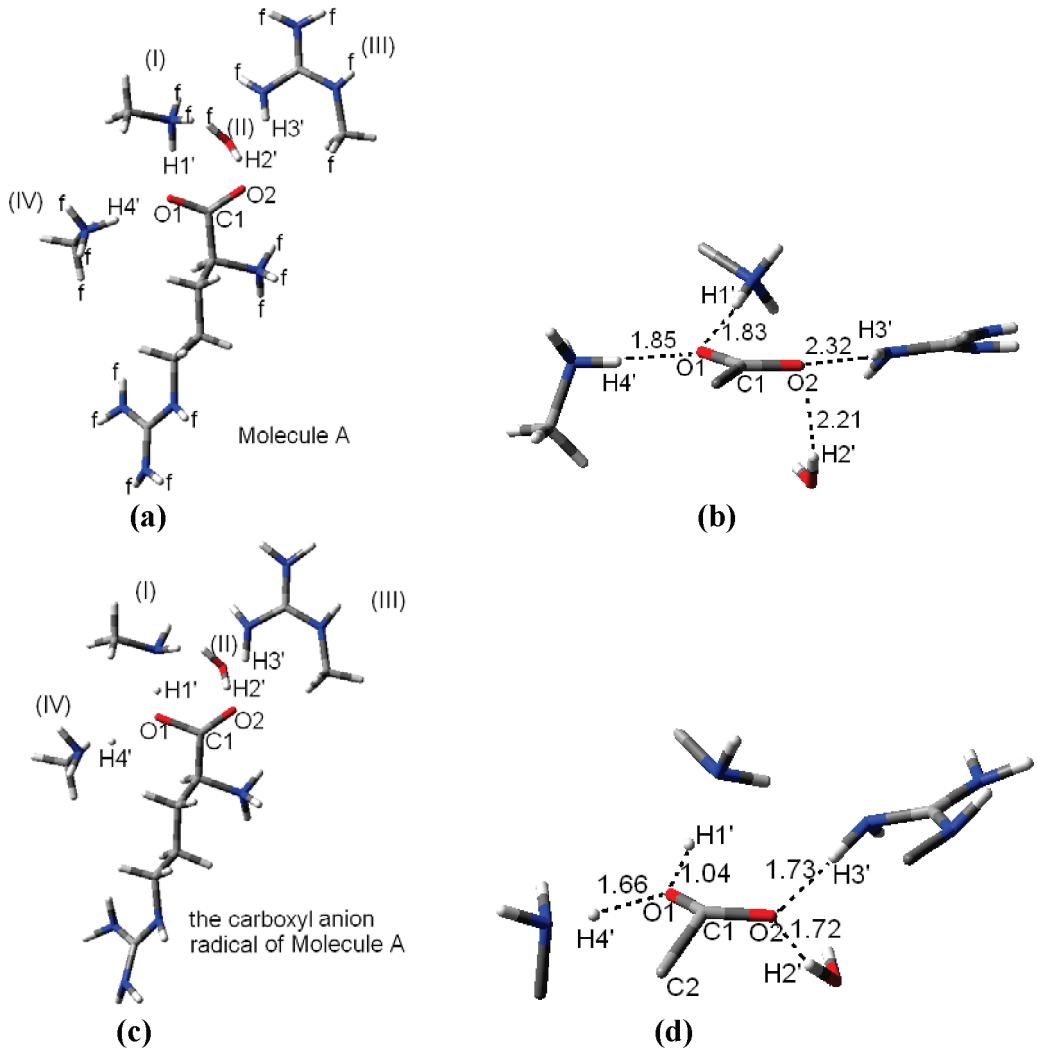

Figure 2. Cluster model for the carboxyl-centered radical from molecule A before (a) and after (c) the geometry optimization. Changes in carboxyl group geometry and hydrogen bond distances are evident by comparing the details shown in (b) (before) and (d) (after) radical formation. The numbers in (b) and (d) are the corresponding hydrogen bond distances in angstroms. The "f"s in (a) mark the atoms frozen during the geometry optimization.

a2 and a3 show characteristics of O−H β-couplings, which have greater anisotropy than typical C−H or N−H β-couplings.[18,19] This behavior also is consistent with the evidence that a2 and a3 are from exchangeable protons. The only reasonable possibility for R1a is the carboxyl-centered radical from one-electron reduction of the parent (see Chart 3), in which the spin is located mainly on C1. For this radical structure, H4 provides the C−H β-coupling a1, while H1′ and H2′ will give the two O−H dipolar couplings a2 and a3. (As shown in Figure 2, H1′ and H2′ are protons from neighboring molecules hydrogen bonded to O1 and O2 of molecule A in the crystal. From the analysis below, H1′ is from the main-chain amino group of a nearby molecule, and H2′ is from an adjacent water molecule.)

Eigenvectors*[20] of tensors a1−a3 were compared to the corresponding crystallographic directions as listed in Table 1. The assignment of coupling a1 to proton H4 is supported by the small difference, less than 7°, between the eigenvector* of a1 and the direction of C1...H4 in molecule A. Similarly, a2 and a3 were assigned to H1′ and H2′, respectively, because the directions of H1′···C1 and H2′···C1 are closest to the eigenvectors* of a2 and a3, respectively. Although the preceding discussion indicated that R1a is the carboxyl-centered radical, the analysis does not provide a distinction between molecules A and B. However, the following geometry-based analysis indicates that R1a is the radical from molecule A.

From the Heller−McConnell equation,[21]

$$a_{C-H} = B_1 \rho \cos^2 \theta \qquad (1)$$

where a_{C-H} is the isotropic value from a C−H β-coupling, B_1 is the constant, ρ is the spin density, and θ is the dihedral angle between the two planes containing the C−H_β bond and the unpaired spin−orbital. With the standard $B_1\rho$ value of 77.3 MHz for the carboxyl-centered reduction radical[22] and the measured isotropic value for a1, the dihedral angle θ is evaluated as 34.2°. For the undamaged molecule A, the torsion angle ∠H4−C2−C1−O1 is 57.8°; if the spin−orbital is normal to the carboxyl plane, the dihedral angle will be 32.2°. This is very close to the calculated dihedral angle for a1. However, torsion angle ∠H4−C2−C1−O1 in undamaged molecule B is 36.3° and gives the dihedral angle 53.7°, which is quite different from the above calculated angle of a1. (It will be shown below that the coupling of radical R1b is more consistent with the geometry of the carboxyl-centered radical from molecule B.)

The $B_1\rho$ value in the Heller−McConnell equation (1) is 40.32 MHz for the O−H dipolar coupling in the carboxyl-centered

TABLE 2: Hyperfine Coupling Tensors Calculated from the Optimized Cluster Model of the Carboxyl-Centered Radical from Molecule A with the Carboxyl Group Adjusted As Described in the Text and Their Comparison to the Experimental Eigenvectors[a,b]

proton	principal value[a]	isotropic value[a]	anisotropic value[a]	eigenvectors a	eigenvectors b	eigenvectors c*	coupling	angle diff (deg)[b]
H4	53.64	45.10	8.54	0.075	0.525	−0.848	:a1	1.1
	41.06		−4.04	−0.043	0.851	0.523		
	40.61		−4.49	0.996	−0.003	0.086		
H1′	25.5	10.28	15.22	0.153	−0.234	−0.960	:a2	5.9
	4.43		−5.85	0.257	0.948	−0.190		
	0.84		−9.44	0.954	−0.218	0.205		
H2′	11.76	−4.90	16.66	0.861	−0.504	−0.07	:a3	1.5
	−12.76		−7.86	0.496	0.801	0.335		
	−13.7		−8.80	−0.113	−0.324	0.940		
H3′	9.47	0.59	8.88	−0.663	−0.311	0.681		
	−3.51		−4.10	0.732	−0.460	0.502		
	−4.19		−4.78	0.160	0.831	0.533		
H4′	6.5	0.67	5.83	0.528	0.846	0.072		
	−1.88		−2.55	0.803	−0.470	−0.367		
	−2.61		−3.28	0.277	−0.251	0.928		
N1	3.85	3.34	0.51					
	3.12		−0.22					
	3.05		−0.29					

[a] Values in MHz. [b] "Angle diff (deg)" are the angular differences between the calculated and the experimental eigenvectors associated with the maximum eigenvalues in degrees.

radical.[18] From this and the isotropic values for a2 and a3, their respective dihedral angles are 61.3° and 78.2°, respectively. These indicate that the two neighboring protons giving a2 and a3 are very close to the nodal plane of the radical. Assuming that the nodal plane is the carboxyl plane in the crystal H1′ is very close to the carboxyl plane (torsion angle ∠H1′−O1−C1−O2 = 21.7°), while H2′ is out of the carboxyl plane by ∼70°. However, the computational modeling discussed below indicates that electron capture leads to the carboxyl group becoming tetrahedral with O2 bending toward H2′, which causes H2′ to move closer to O2. These geometric changes in the radical bring H2′ much closer to the nodal plane (see Figure 2d), thereby causing a small isotropic value.

3.2. Cluster Modeling Calculations for R1a. The cluster model used for computational investigation of R1a is shown in Figure 2a. It was constructed on the basis that molecule A is the neighbor to four groups I−IV. Groups I and IV are the main chain amino groups in two different neighboring arginine molecules, group III is the side chain guanidyl group of a third arginine neighbor, and group II is a neighboring water molecule. The remainders of the molecules in groups I, III, and IV are simplified by three methyl groups. In these four neighboring groups, H1′ of I and H4′ of IV are hydrogen bonded to O1 while H2′ of II and H3′ of III are hydrogen bonded to O2. For the computation, one electron was added to the whole cluster and the environmental effects were simulated by freezing some of the atoms in the cluster model during the geometry optimization, as indicated by the atoms labeled "f" in Figure 2a. Except for the methyl groups, all atomic coordinates in the cluster, including the hydrogens, came from the crystallographic study.[11]

The partially optimized cluster is shown in Figure 2c. (The optimization was "partial" as a result of the frozen coordinates.) The carboxyl group of molecule A has a tetrahedral structure (see Figure 2d) with torsion angle ∠C2−O2−O1−C1 of 29.2°, a significant rearrangement from the planar structure before the optimization. Also, protons H1′−H4′ are closer to the carboxyl group than in the parent structure. The single point calculation indicates that the spin density is mainly located on he carboxyl group, C1 (0.66), O1 (0.04), and O2 (0.19). As listed in Table 2, the hyperfine tensors calculated from protons H4, H1′, and H2′ reproduce the experimental tensors a1, a2, and a3 very well. These results confirm the assignment of R1a as the carboxyl-centered radical from molecule A with a C−H β-coupling a1 from H4 and two O−H dipolar couplings a2 and a3 from H1′ and H2′, respectively. The optimized geometry shown in Figure 2c,d also indicates that H1′ was transferred to O2 through the hydrogen bond from the neighboring molecule as a result of the electron capture: the distance O1...H1′ shortened from 1.83 to 1.04 Å, and the distance N′(I)...H1′ lengthened from 0.95 to 1.53 Å. Upon geometry optimization, the whole water molecule containing H2′ moved closer to the carboxyl group as a result of electron trapping. Protons H3′ and H4′ also moved closer to the carboxyl group (shortening ∼0.6 Å for H3′...O2 and ∼0.2 Å for H4′...O1). Tensor a3 was assigned to H2′ (and not H3′ or H4′) on the basis that its computed anisotropic components and eigenvectors correspond best to the measured values. The computed couplings from H3′, H4′, and N1 (a β-coupling) are consistent with the assumption that they were too small to be detected in the experiments.

3.3. Radical R1b: Carboxyl-Centered One-Electron Reduction Radical from Molecule B. As is shown in Figure 1 (upper left) ENDOR lines b1−b3 from normal crystals gave strong one-peak EIE patterns for B//*c* and were assigned to radical R1b. WINSIM simulations indicate that couplings b1−b3 are small and unresolvable in the R1b EIE patterns. The presence of line b1 in ENDOR spectra from partially deuterated crystals at *c* and the absence of lines b2 and b3 indicate that b1 is from a nonexchangeable hydrogen, while b2 and b3 are from exchangeable ones. The hyperfine coupling tensor from b1 is listed in Table 1; unfortunately, ENDOR lines b2 and b3 overlapped with the free proton lines at most orientations and

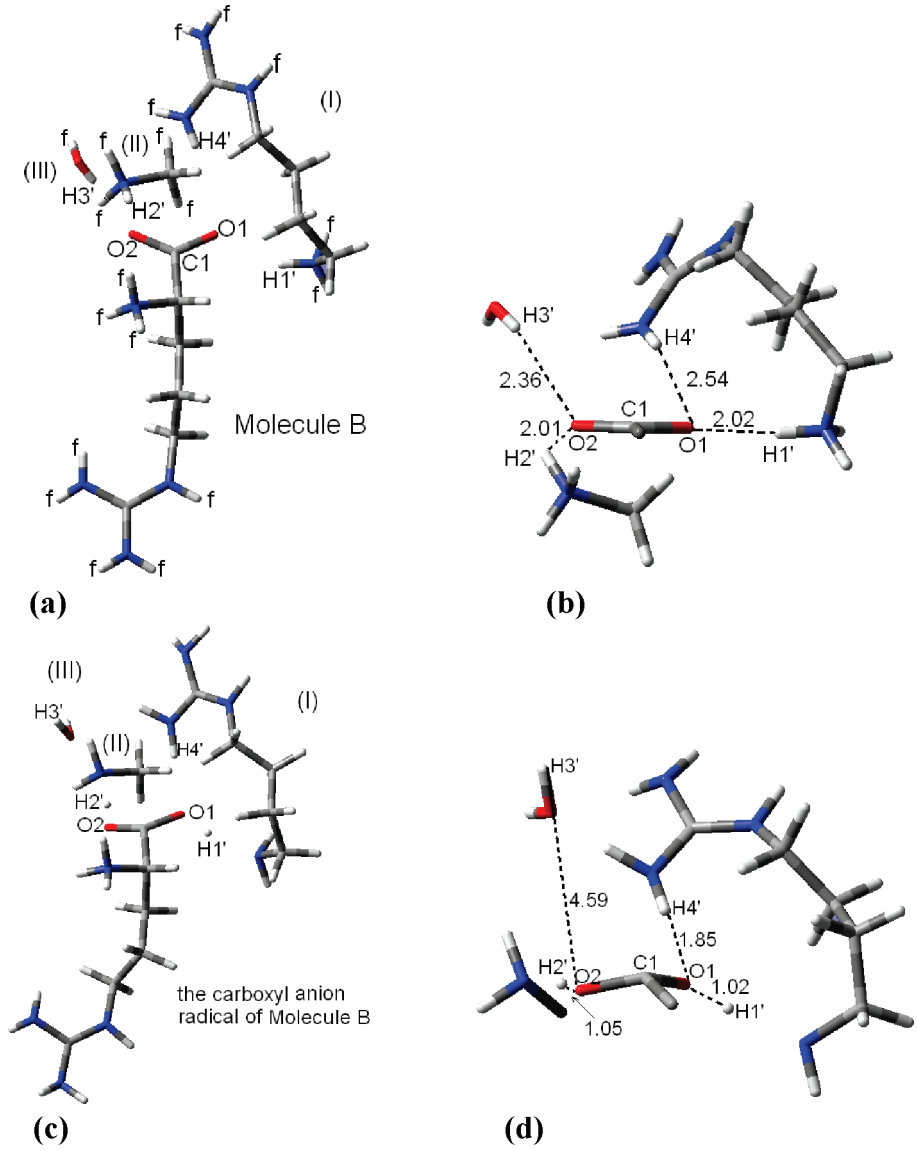

Figure 3. Cluster model for the carboxyl-centered radical from molecule B before (a) and after (c) the geometry optimization. Changes in carboxyl group geometry and hydrogen bond distances are evident by comparing the details shown in (b) (before) and (d) (after) radical formation. The numbers in (b) and (d) are the corresponding hydrogen bond distances in the units of angstroms. The "f's in (a) mark the frozen atoms during the geometry optimization.

it was not possible to obtain their tensors. Coupling b1 shows moderate anisotropy, and because it is nonexchangeable, it was assigned to a C−H β-coupling.

R1b apparently is a carboxyl-centered one-electron reduction radical (see Chart 3) in a conformation different from R1a in which the C−H β-coupling b1 is the result of H4. The isotropic coupling of b1 is much smaller than that of a1 in R1a. The Heller−McConnell equation (1) for C−H β-couplings indicates the dihedral angle for b1 is 68.3° (with $B_1\rho$ = 77.3 MHz). Assuming spin−orbitals normal to the carboxyl planes of undamaged molecules A and B, crystallographic data indicate respective dihedral angles for H4 of 32.2° and 53.7°. Thus, the dihedral angle for b1 from eq 1 is near that of H4 in undamaged molecule B but is almost twice of that in molecule A. In addition, the eigenvector* of b1 is almost parallel to the crystallographic direction C1...H4 in molecule B, as shown in Table 1. Therefore, it is reasonable to assign b1 to proton H4 in molecule B and exchangeable couplings b2 and b3 to the protons associated with the carboxyl oxygen atoms. Because b1 and b2 are small, they apparently arise from a proton very near the nodal plane of the spin−orbital. Protons H1′−H4′, shown in Figure 3b, associate with the carboxyl group of molecule B. For the parent molecule, their respective torsion angles to the carboxyl plane are ∠H1′−O1−C1−O2 = 1.5°, ∠H2′−O2−C1−O1 = 31.1°, ∠H3′−O2−C1−O1 = 86.7°, and ∠H4′−O1−C1−O2 = 40.1°. The modeling calculations discussed below indicate that H1′ and H2′ give b1 and b2 the O−H dipolar couplings of the radical.

3.4. Cluster Modeling Calculations for R1b. The cluster model for the carboxyl-centered radical of molecule B included its three neighboring groups: group I is a truncated arginine molecule with the main chain carboxyl group replaced by a hydrogen atom, group II is the main chain amino group of a different neighboring arginine molecule with the remainder replaced by a methyl group, and group III is a neighboring water molecule. H1′ and H4′ are in group I and are hydrogen bonded to O1; H2′ in II and H3′ in III are hydrogen bonded to O2. Similar to the case with R1a, an electron was added to the whole cluster and some of the atoms were fixed during the optimization

TABLE 3: Hyperfine Coupling Tensors Calculated from the Optimized Cluster Model of the Carboxyl-Centered Radical from Molecule B with the Carboxyl Group Adjusted As Described in the Text and Their Comparison to the Experimental Eigenvectors[a,b]

proton	principal value[a]	isotropic value[a]	anisotropic value[a]	eigenvectors			coupling	angle diff (deg)[b]
				a	*b*	*c**		
H4	22.78	11.83	10.95	0.236	0.550	−0.801	:b1	11.0
	7.54		−4.29	0.971	−0.168	0.171		
	5.18		−6.65	0.041	0.818	0.574		
H1′	10.41	−4.53	14.94	0.392	0.913	−0.111		
	−9.72		−5.19	0.65	−0.19	0.736		
	−14.28		−9.75	−0.651	0.361	0.668		
H2′	16.43	−7.27	16.43	0.015	−0.307	0.952		
	−6.47		−6.47	0.831	−0.526	−0.183		
	−9.96		−9.96	0.556	0.793	0.248		
H3′	1.64	−0.03	1.67	0.899	0.432	0.076		
	−0.81		−0.81	−0.318	0.76	−0.567		
	−0.86		−0.86	−0.303	0.486	0.82		
H4′	9.07	0.89	8.18	−0.561	0.306	0.769		
	−3.21		−3.21	0.773	0.525	0.355		
	−4.97		−4.97	−0.295	0.794	−0.531		
N1	15.26	14.19	1.06	−0.205	0.424	0.882		
	−0.45		−0.45	−0.414	0.779	−0.471		
	−0.62		−0.62	0.887	0.461	−0.016		

[a] Values in MHz. [b] "Angle diff (deg)" are the angular differences between the calculated and the experimental eigenvectors associated with the maximum eigenvalues in degrees.

to simulate the environmental effects. (The fixed atoms are marked "f" in Figure 3a.)

Upon geometry optimization, the planar carboxyl group of molecule B became tetrahedral with a torsion angle ∠O1−C2−O2−C1 of 22.6° upon electron trapping (see Figure 3c,d). Meanwhile, protons H1′ in group I and H2′ in II moved closer to O1 and O2 (distances H1′···O1 of 1.02 Å and H2′···O2 of 1.05 Å) and farther from their original groups (distance N1′(I)···H1′ from 0.89 to 1.71 Å, and N′(II)···H2′ from 0.91 to 1.62 Å). These indicate that protons H1′ and H2′ transferred to O1 and O2 upon electron trapping.

Single point calculations performed on the optimized cluster model indicate that the spin density is mainly on the carboxyl group: $\rho(C1) = 0.71$, $\rho(O1) = 0.07$, and $\rho(O2) = 0.15$. The calculated coupling tensor from H4 is approximately the same as b1. However, the calculated coupling from H1′ is 16.60 MHz, which is too large for coupling b2 or b3. To investigate this apparent overestimate further, the carboxyl group was rotated manually about the C1−C2 axis by ∼10°. The hyperfine coupling tensors from the adjusted structure, listed in Table 3, are in good agreement with the experimental results. Although it was not possible to measure tensors b2 and b3, the calculated tensors from H1′ and H2′ approximately reproduce the angular dependence curves of b2 and b3 detected in *ac* plane (see Figures S2 and S3 of the Supporting Information). Also, the EIE pattern of R1b can be reproduced well by using the calculated couplings for protons H4, H1′−H4′, and N1. On the basis of these results, we assigned coupling b2 to proton H1′ and b3 to H2′ and concluded that R1b is the result of electron trapping by molecule B with coupling b1 from proton H4, b2 from H1′, and b3 from H2′.

3.5. Radical R2: Decarboxylation Radical. Weak ENDOR lines A−D gave six-line EIE patterns (B//*c*) for the normal crystal with peak ratios of 1:2:2:2:2:1 (Figure 1 left) and were assigned to radical R2. Their hyperfine coupling tensors are listed in Table 4. The anisotropic components of tensor A are typical of a C−H α-coupling (nonexchangeable), and tensors B−D are β-couplings. Simulations using tensors A−D reproduce the EIE patterns of R2 from normal crystals at three crystallographic axes. The ENDOR spectrum for B//*c* from the partially deuterated crystal (Figure 1 right) shows that coupling C is from a nonexchangeable proton. It was not possible to confirm whether couplings B and D were from exchangeable or nonexchangeable proton because they were very weak in the ENDOR spectra from both types of crystal. However, the EIE pattern from ENDOR line C at B//*c* for the partially deuterated crystal is a three-line pattern with peak ratio of 1:2:1 (Figure 1 right). This pattern can be simulated with couplings A and C alone, thereby indicating that couplings B and D are from exchangeable protons.

From these results, R2 can only be the decarboxylation radical (Chart 4) for which the spin is mainly on C2, H4 is a C−H α-proton, H1−H3 are exchangeable β-protons, and H5 and H6 are nonexchangeable protons. As shown in Table 5, the eigenvector* couplings B−D approximate well the corresponding crystallographic directions of a decarboxylated structure in molecules A and B. (We note that eigenvectors* of tensors B and C are different by only 2.5°, and both are close to directions H1...C2, H5...C2, and H6...C2. Coupling B is from an exchangeable proton and was ascribed to H1 while coupling C was attributed to nonexchangeable proton H5 or H6). The eigenvector associated with the positive anisotropic component of α-coupling A is ∼30° different from direction H4−C2 in molecules A and B. These results for the β-protons indicate that they reoriented very little as the radical was formed, while the α-coupling indicates greater rearrangement of the radical center. These also were characteristics of the decarboxylation radicals in irradiated L-lysine hydrochloride dihydrate[6] and L-*O*-serine phosphate.[23] Apparently, the hydrogen bonds of the main chain amino protons and the guanidyl protons fix the radical and restrict its movement. Thus, the main reorientation is the

TABLE 4: Hyperfine Coupling Tensors for Radical R2[a,b]

coupling	principal value[a,b]	isotropic value[a,b]	anisotropic value[a,b]	eigenvector[b]		
				a	*b*	*c**
A	−82.99(3)	−47.95	−35.04	0.776(1)	0.445(0)	0.447(0)
	−47.84(3)		0.11	0.419(0)	0.166(1)	−0.893(0)
	−13.02(3)		34.93	0.472(1)	−0.880(0)	0.058(1)
B	59.73(2)	47.68	12.05	0.835(0)	0.483(1)	0.264(5)
	42.43(2)		−5.25	0.550(0)	−0.736(4)	−0.394(6)
	40.89(2)		−6.79	0.005(1)	0.474(8)	−0.880(3)
C	62.59(2)	53.30	9.29	0.811(1)	0.511(12)	0.286(25)
	48.80(2)		−4.50	0.531(1)	−0.436(36)	−0.727(21)
	48.51(2)		−4.79	0.246(1)	−0.741(30)	0.624(35)
D	89.84(2)	80.20	9.64	−0.301(1)	−0.097(1)	−0.949(0)
	79.36(2)		−0.84	0.377(1)	−0.926(0)	−0.025(1)
	71.41(2)		−8.79	0.876(0)	0.365(1)	−0.315(1)

[a] Values in MHz. [b] Numbers in parentheses are the estimated uncertainties in the respective values as reported by the statistical analysis.

TABLE 5: Comparisons between the Eigenvectors[a] of Couplings A−D and the Corresponding Crystallographic Directions Related to the Decarboxylation Radical from Molecules A and B[b,c]

couplings	eigenvectors[a]			protons	directions of Hx...C2 in MA			angle diff (deg)[b]
	a	*b*	*c**		*a*	*b*	*c**	
A	0.472	−0.88	0.058	H4	0.203	−0.89	0.408	25.5
B	0.835	0.483	0.264	H1	0.760	0.557	0.336	7.1
C	0.811	0.511	0.286	H1	0.760	0.557	0.336	4.4
B	0.835	0.483	0.264	H5	0.823	0.512[c]	0.245	2.3
C	0.811	0.511	0.286	H5	0.823	0.512[c]	0.245	2.4
B	0.835	0.483	0.264	H6	0.912	0.262	0.316	13.7
C	0.811	0.511	0.286	H6	0.912	0.262	0.316	15.4
D	0.301	0.097	0.949	H2	0.326	0.363	0.873	15.9
couplings	eigenvectors[a]			protons	directions of Hx...C2 in MB			angle diff (deg)[b]
	a	*b*	*c**		*a*	*b*	*c**	
A	0.472	−0.880	0.058	H4	0.069	−0.93	0.362	29.3
B	0.835	0.483	0.264	H1	0.842	0.360	0.402	10.6
C	0.811	0.511	0.286	H1	0.842	0.360	0.402	10.9
B	0.835	0.483	0.264	H5	0.720	0.641[c]	0.266	11.2
C	0.811	0.511	0.286	H5	0.720	0.641[c]	0.266	9.1
B	0.835	0.483	0.264	H6	0.956	0.089	0.279	23.8
C	0.811	0.511	0.286	H6	0.956	0.089	0.279	25.8
D	0.301	0.097	0.949	H2	0.301	0.301	0.905	11.9

[a] The eigenvectors are those associated with the maximum coupling components. [b] "Angle diff (deg)" are the angular differences between the experimental eigenvectors and the crystallographic directions in units of degrees. [c] The sign of the *y* component is changed from "−" to "+" due to the symmetry of the monoclinic system.

rehybridization of the radical center C2 from sp^3 to sp^2, with the consequence that the direction H4−C2 is significantly reoriented.

The extent of rehybridization, and residual bending at the radical center, is indicated by comparison of results from the McConnell relation[24]

$$a_{iso}(\mathbf{H}\alpha) = \mathbf{Q}\rho \tag{2}$$

and the Gordy−Bernhard relation,[25,26]

$$a_z = \mathbf{Q}^z_{dip}\rho \tag{3}$$

Using the isotropic value of coupling A with $Q = -73.4$ MHz,[27] eq 2 indicates $\rho = 0.65$; using the positive anisotropic component of α-coupling A with $Q^z_{dip} = 38.7$ MHz,[25] eq 3 indicates $\rho = 0.90$. That these values are different indicates that the radical center did not fully attain the sp^2 configuration and that the C2−H4 bond does not lie in the C2−N3−C3 plane.[28] This condition is reproduced by the modeling computations described below.

To a first approximation, it is reasonable to assume that the orbital of the unpaired electron in R2 parallels the C2−C1 bond of molecules A and B in the undamaged crystal. From the crystallographic data, the C2−C1 bond makes dihedral angles with the β-protons of ∼38°(H1), ∼25°(H2), ∼85°(H3), ∼53°(H5), ∼62°(H6). From these and relation 1, a qualitative estimate for the β-proton couplings is that H2 should have the largest coupling, that H3 and H6 should have much smaller couplings, and that H1 and H5 should have moderate couplings. These are consistent with the analysis above based on dipolar directions: coupling D is largest and its eigenvector* is approximately parallel to H2···C2; couplings B and C are moderate, and their eigenvectors* are approximately parallel to directions H1···C2 and H5···C2, respectively. There was

TABLE 6: Calculated Hyperfine Coupling Tensors from the Final Models for the Decarboxylation Radical from Molecule A[a,b]

			eigenvectors				
proton	isotropic value[a]	anisotropic value[a]	*a*	*b*	*c**	: coupling	angle diff (deg)[b]
		12.50	0.692	0.597	0.407	:B	13.2
H1	62.61	−5.92	0.721	−0.535	−0.441		
		−6.58	−0.045	0.598	−0.800		
		8.61	−0.411	−0.324	−0.852	:D	15.5
H2	88.26	−3.22	0.396	−0.905	0.153		
		−5.39	0.821	0.275	−0.500		
		9.32	−0.050	0.791	0.609		
H3	0.83	−3.89	0.218	−0.587	0.780		
		−5.43	0.975	0.172	−0.143		
		−36.67	0.760	0.420	0.496		3.3
H4	−41.43	−4.70	0.480	0.151	−0.864	:A	3.9
		41.37	0.438	−0.895	0.087		2.0
		10.76	0.879	−0.406	0.250	:C	7.3
H5	63.4	−5.11	0.466	0.842	−0.271		
		−5.65	−0.100	0.355	0.930		
		10.06	0.822	0.460	0.336		
H6	5.46	−4.50	−0.216	−0.294	0.931		
		−5.56	−0.527	0.838	0.143		

[a] Values in MHz. [b] "Angle diff (deg)" are the angular differences between the calculated and the experimental eigenvectors in degrees.

no detectable experimental data potentially from H3 and H6, but this is consistent with their larger dihedral angles and the likelihood that their couplings were too small to be detected. Therefore, all analyses based on the experimental data support the assignment of R2 to the decarboxylation radical.

3.6. Modeling Calculations for R2. None of the protons implicated by analysis of the experimental data for R2 involved neighboring molecules. For that reason the computational model was constructed as single molecules from coordinates of A and B units,[11] and with the carboxyl groups removed. However, environmental effects were introduced in two ways: (1) The PCM model[29] was used in the geometry optimization with the dielectric constant of water (78.39); (2) the three main chain amino protons were frozen during the PCM optimizations because the analysis above indicates little reorientation of the β-protons. However, the calculated β-couplings are different from the experimental ones by more than 15 MHz. Single point calculations on the optimized structures indicate spins of 0.90 on C2 of molecules A and B. Also, for both, eigenvectors of the tensors calculated for H4, H1, H5, and H2 closely approximate those of tensors A, B, C, and D, respectively. However, the computed α-coupling parameter from H4 is larger than coupling A by more than 15 MHz. Although the experimental data indicated residual sp^3 character of the bonds to C2, the optimized radical centers were purely planar at C2 with the torsion angle ∠C3−N1−H4−C2 of ∼10° for molecules A and B. In seeking a radical geometry with calculated couplings that better matched experimental results, three adjustments were performed manually on the optimized radical structure from molecules A and B: (1) bending H4 by 20° out of the C3−C2−N1 plane; (2) rotating the main chain amino protons about the N1−C2 axis by ∼15°; (3) rotating the whole side chain about the C2−C3 axis by 20°. These operations greatly improved the correspondence between the computed and experimental results as is shown in Table 6. Results from computations based on the structure of molecule B were virtually identical; see Table S1 of the Supporting Information.) Therefore, the modeling calculations support the identification of R2 to the decarboxylation radical and indicate that the radical within the crystal was restricted from reorienting as much as the computations suggest.

3.7. Radical R3: Guanidyl-Centered One-Electron Reduction Radical. ENDOR lines 1 and 2 from the normal crystal gave five-line EIE patterns (B//*c*) with approximate peak ratios 1:1:2:1:1 (Figure 1 upper left) and were assigned to R3. At all three crystallographic axes EIE patterns from R3 are wider than the corresponding sums of couplings 1 and 2 by ∼72 MHz (∼26 G), a result indicating additional couplings totaling ∼72 MHz not detected initially by ENDOR. We explored two possibilities for these: (a) one $I = 1$ species with coupling approximately 36 MHz and (b) two $I = {}^1/_2$ species with couplings summing to approximately 72 MHz. From WINSIM simulations, as shown in the upper part of Figure 4, the EIE pattern for B//*c* was reproduced very well (width and approximate peak ratios) by supplementing couplings 1 and 2 with an $I = 1$ coupling of 37.38 MHz. As shown in the lower part of Figure 4, the simulation using two $I = {}^1/_2$ couplings each of ∼36.40 MHz reproduced the EIE's width well but not the peak ratios. In addition, simulations using an $I = 1$ coupling of ∼37 MHz also reproduced the EIE patterns at the other two axis positions (see Figure S7 of the Supporting Information). On the basis of the indications from the simulations, we sought ENDOR evidence for a virtually isotropic nitrogen coupling of ca. 37 MHz and detected the lines for B//*a* (coupling ∼43 MHz) and B//*c* (coupling ∼38.8 MHz; see the Supporting Information for more detail). Therefore, the ENDOR results confirm the conclusion from the WINSIM simulations that coupling 3, of ∼37 MHz at all three axes, is from a nitrogen.

Hyperfine coupling tensors 1 and 2 are listed in Table 7; both are characteristic of β-couplings. As shown in Figure 1 right, lines 1 and 2 were absent in ENDOR spectra from the partially deuterated crystals. This indicates that both couplings are from exchangeable protons, i.e., protons bonded to nitrogen or oxygen atoms. However, coupling 1 is unlikely to be from an O−H β-proton: its anisotropic values are smaller than those of typical O−H dipolar couplings, its isotropic value of 93.26 MHz is

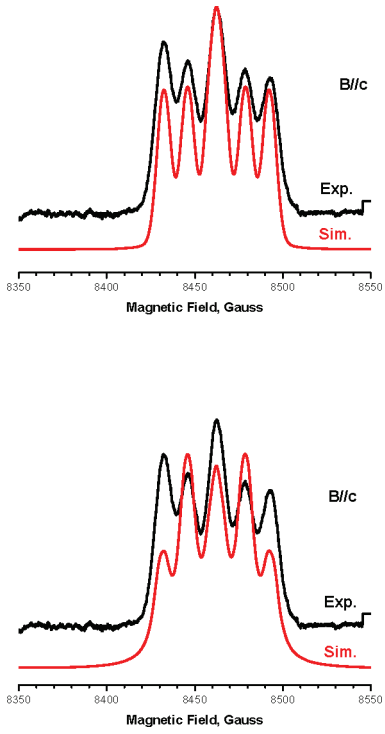

Figure 4. WINSIM simulations of EIE patterns from R3 in the normal crystal for B//*c*. In the upper figure, one nitrogen coupling was set as that missing from the ENDOR set, and in the lower figure, two proton couplings were set as those missing.

much larger than those of the O−H dipolar couplings in R1a and R1b (<10 MHz), and its eigenvector* is very different from the crystallographic directions C1...H*x*′ in molecules A and B shown in Table 1. (H*x*′ are the protons H1′−H4′ hydrogen bonded O1 and O2 in molecule A and B, as shown in Figures 2 and 3.) Therefore, coupling 1 was assigned as that from a N−H β-proton. In arginine (Chart 1), the nitrogen atoms are at least three bonds away from oxygen; thus, coupling 2 cannot be from an O−H β-proton if coupling 1 is from a N−H β-proton. In summary, we conclude that both couplings 1 and 2 are from N−H β-protons.

These characteristics suggest two possibilities for R3. One is the H4 abstraction product (see Chart 6) with the spin mainly located on C2. In this structure, two of three main-chain amino β-protons and the α-nitrogen in this radical could provide couplings 1−3, and the geometry could be such that the remaining couplings are too small to be detected, i.e., if the corresponding protons are very close to the nodal plane of the radical. We found that the H4 dehydrogenation radical was identified as one of the stable radicals in L-arg·HCl·H_2O crystals irradiated at room temperature.[30] In our experiments, this radical exhibited a large nonexchangeable (C−H) β-coupling with isotropic value greater than 100 MHz and virtually no nitrogen coupling. Therefore, we concluded that R3 is unlikely to be the radical from H4 abstraction.

The other possibility for R3 is the "guanidyl anion" radical (see Chart 7), the result of one-electron reduction like R1a and R1b but with the unpaired spin mainly resident on atom C6 of the guanidyl group. Such a structure can exhibit five N−H β-couplings and three α nitrogen couplings. Table 7 lists crystallographic directions of Hx···C6 (x = 11, 12, ..., 0.15, respectively) in both molecules A and B. The eigenvectors* of both couplings 1 and 2 closely approximate the directions H11···C6 and H13···C6 in molecules A and B. (We note that the directions H11···C6 and H13···C6 are similar, and that the eigenvectors* of couplings 1 and 2 also are similar.) Thus, these comparisons indicate that couplings 1 and 2 might arise from protons H11 and H13, but they do not allow assigning the couplings to specific protons. Also, the couplings might be from protons of molecules A and B, or the two cases might be indistinguishable. To investigate these possibilities further, we carried out a series of modeling calculations, as described below, and found that they supported the identification of R3 as the guanidyl-centered one-electron reduction radical.

3.8. Cluster Modeling Calculations for R3. Cluster models for investigating guanidyl-centered radicals from molecules A and B were built from crystallographic coordinates and the molecular packing in the L-arg·HCl·H_2O crystals.[11] As shown in Figure 5a, the cluster for molecule A includes the central molecule and portions of three neighboring molecules with which it interacts by hydrogen bonding. The neighboring molecules are two waters (groups I and II) and a truncated version of another arginine molecule (group III) consisting of the main chain units (the carboxyl group, the amino group, the α-carbon, and the α-hydrogen) with the remainder of the molecule replaced by a hydrogen atom. Oxygen atoms in I and II are hydrogen bonded to H15 and H16, respectively, while O1′ and H3′ in III are hydrogen bonded to H12 and O1, respectively, of the central molecule. (H11 and H13 of molecule A in the crystals also are hydrogen bonded to two different Cl^- ions, but these were omitted in the model.)

One electron was added to the whole cluster to simulate the radical. During geometry optimization, some atoms were frozen (marked "f" in Figure 5a) to simulate additional crystallographic environmental effects, but the guanidyl group and the side chain of the center molecule were fully optimized. The optimized cluster for molecule A is shown in Figure 5b. The most evident geometric change is that the guanidyl group changed from planar to tetrahedral with the torsion angle ∠N2−N4−N3−C6 = 22.8°. The subsequent single point calculation indicated that the spin mainly localized onto C6 (0.72). The calculated coupling tensor for H13 is similar to measured tensor 1. However, no calculated tensors compare well to measured tensor 2. Also, the calculation indicates two large nitrogen couplings, of 61.33 MHz from N2 and 46.13 MHz from N3, and these are inconsistent with the experimental results that indicate only one large nitrogen coupling (∼36 MHz). Because the Cl^- was omitted in the cluster model and H11 was unconstrained in the optimization, the H11...Cl^- hydrogen bond was not well-represented in the optimized model. Consequently, the N2−H11 bond was bent manually toward the direction of H11...Cl^- by ∼30° (see Figure 5c). With this change, the tensors calculated for H13 and H11 agreed well with experimental tensors 1 and 2. Also, the adjusted structure exhibited only one large nitrogen coupling of 40.29 MHz from N3, a result in good agreement with experimental coupling 3 (∼36 MHz). However, the coupling of 25.91 MHz computed for H14 in the adjusted model has no experimental counterpart. Thus, as a final step, the positions of H14 and H15 were rotated manually about the C6−N4 axis by 15°. Tensors calculated from the final adjusted model are listed in Table 8. These show that the calculations for H13 and H11 agree well with experimental tensors 1 and 2, that the coupling calculated for N3 agrees well with coupling 3, and that the couplings computed for H14 and H15 are acceptable.

A similar procedure based on the coordinates and packing of molecule B led to similar results. Upon optimization, the originally planar guanidyl group became tetrahedral with torsion angle ∠N2−N4−N3−C6 of 25.5°; the single point calculation

TABLE 7: Hyperfine Coupling Tensors for Radical R3 and the Comparisons between the Eigenvectors* of Couplings 1 and 2 and the Crystallographic Directions Related to the Guanidyl-Centered Radical in Molecules A and B[a,b]

coupling	principal value[a,b]	isotropic value[a]	anisotropic value[a]	eigenvector[b] *a*	*b*	*c**
1	99.98(2)	93.26	6.72	0.069(1)	−0.926(3)	−0.370(3)
	91.05(2)		−2.21	0.654(0)	0.322(1)	−0.685(2)
	88.75(2)		−4.51	0.754(1)	−0.195(2)	0.628(3)
2	32.65(2)	17.38	15.27	0.502(1)	−0.864(4)	0.025(2)
	11.13(3)		−6.25	0.376(0)	0.244(2)	0.894(2)
	8.36(2)		−9.02	0.779(1)	0.440(2)	−0.448(5)
3	∼43				along *a*	
	∼38.8				along *c*	

		eigenvector[b] *a*	*b*	*c**
crystallographic directions in MA[c]	H11...C6	−0.131	−0.956	−0.261
	H12...C6	0.632	−0.561	−0.535
	H13...C6	0.210	−0.978	−0.011
	H14...C6	0.728	−0.342	−0.595
	H15...C6	−0.374	−0.362	0.854
crystallographic directions in MB[c]	H11...C6	−0.239	−0.944	−0.229
	H12...C6	0.772	−0.482	−0.414
	H13...C6	0.311	−0.948	−0.068
	H14...C6	0.752	−0.233	−0.617
	H15...C6	−0.400	−0.385	0.832

		angle diff (deg)[e]
eigenvector* of coupling 1[d]	H11...C6 (MA)	13.4
	H13...C6 (MA)	22.5
	H11...C6 (MB)	19.5
	H13...C6 (MB)	22.4
eigenvector* of coupling 2[d]	H11...C6 (MA)	26.1
	H13...C6 (MA)	18.2
	H11...C6 (MB)	18.7
	H13...C6 (MB)	13.2

[a] Values in MHz. [b] Numbers in parentheses are the estimated uncertainties in the respective values as reported by the statistical analysis. [c] The signs of the eigenvector's *y* component can be changed to "+" from "−" due to the symmetry of monoclinic crystal. "MA" and "MB" stand for molecules A and B, respectively. [d] The eigenvector* is that associated with the maximum eigenvalue. [e] "Angle diff (deg)" is the angular difference between the experimental eigenvector* and the crystallographic directions in degrees.

CHART 6: Radical from Dehydrogenation at C2

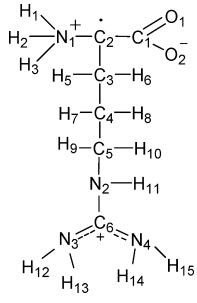

CHART 7: Guanidyl-Centered Radical from One-Electron Reduction

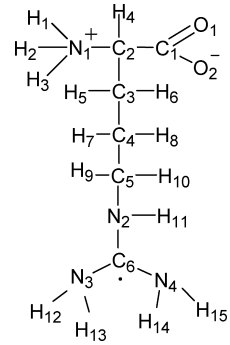

showed spin mainly on C6 (0.73); tensors calculated for H11 and H13 agree well with couplings 2 and 1, respectively; rotation of H12 and H13 manually about the N3−C6 axis by 10° and rotation of H15 and H16 manually about the N4−C6 axis by 5° led to computed values consistent with measurements (see Table S2 of the Supporting Information).

Therefore, the calculations for molecules A and B within the model cluster environment support the assignment of radical R3 as the result of one-electron reduction of arginine with the unpaired electron residing on the guanidyl group. The modeling results indicate that radicals formed on molecules A and B are indistinguishable and that couplings 1−3 arise from H13, H11, and N3, respectively. The couplings calculated for H12, H14, H15, N2, and N4 were not detected experimentally, probably due to their relatively smaller values and overlap with the lines near the free proton signal.

3.9. Radical R4: Dehydrogenation at C5. The EIE pattern from R4 in the normal crystal was observed only for B//*c* and is shown in the upper left panel of Figure 1. The EIE peak ratio of ∼1:1:2:2:2:2:1:1 suggests that more than one coupling contributed to the pattern. However, only one ENDOR line,

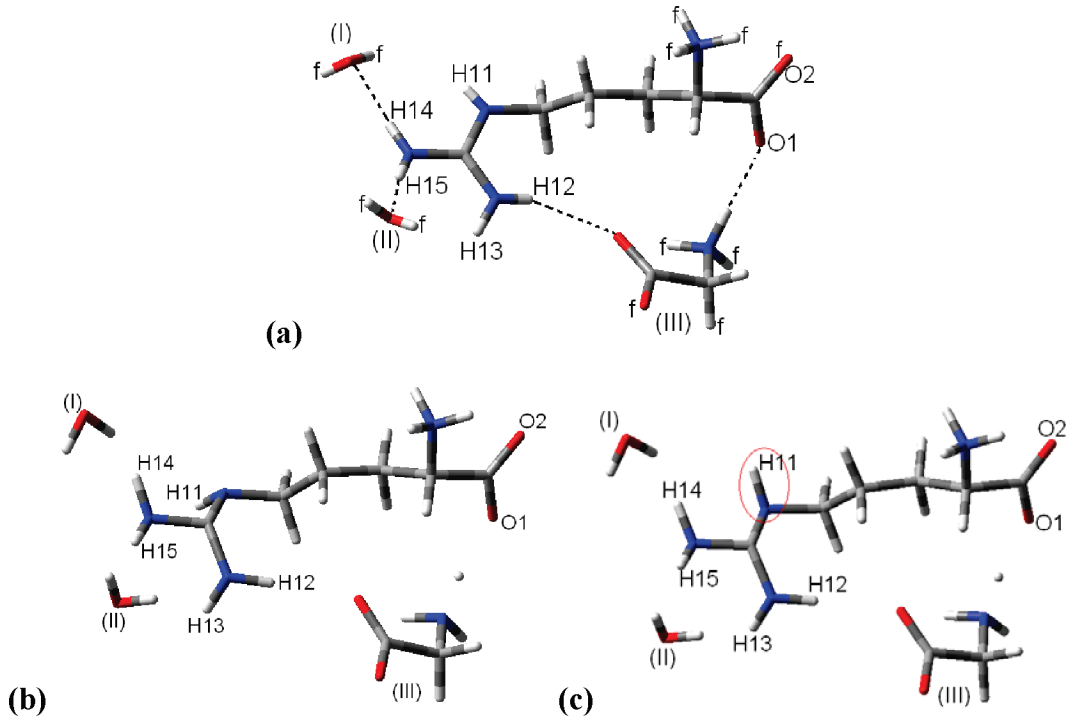

Figure 5. Cluster model for the guanidyl-centered electron adduct of molecule A: (a) cluster before optimization A; (b) initially optimized cluster; (c) cluster model adjusted by bending H11. The dashed lines show the hydrogen bonding, and the atoms frozen during the geometry optimization are marked by "f."

TABLE 8: Calculated Coupling Tensors from the Adjusted Cluster Model for the Guanidyl-Centered Radical from Molecule A[a,b]

			eigenvectors				
proton	isotropic value[a]	anisotropic value[a]	*a*	*b*	*c**	: coupling	angle diff (deg)[b]
		15.1	0.321	−0.945	0.053		11.8
H11	11.64	−5.66	0.481	0.212	0.851	:2	6.6
		−9.45	0.816	0.248	−0.522		11.9
		10.07	−0.449	0.616	0.648		
H12	−1.41	−3.74	0.161	0.769	−0.619		
		−6.33	0.879	0.174	0.444		
		7.13	−0.183	−0.942	−0.280		15.6
H13	105.3	−2.63	0.641	0.102	−0.761	:1	13.3
		−4.50	0.745	−0.319	0.586		7.3
		13.18	−0.668	0.700	0.251		
H14	7.17	−5.07	0.738	0.666	0.108		
		−8.10	0.092	−0.257	0.962		
		12.59	−0.191	−0.477	0.858		
H15	7.62	−4.71	0.960	0.093	0.266		
		−7.88	−0.207	0.874	0.440		
		3.63	0.154	0.209	0.966		
N3	48.09	−1.19	−0.68	0.732	−0.05		
		−2.44	0.717	0.649	−0.255		
N1	0.55						
N2	−1.00						
N4	−1.94						

[a] Values in MHz. [b] "Angle diff (deg)" are the angular differences between the calculated and the experimental eigenvectors in degrees.

denoted as "R4-I", was detected. Hyperfine coupling tensor R4-I is listed in Table 9, and it is a typical C−H α-coupling.

WINSIM simulations indicate that the EIE pattern from R4 (Figure 1 upper left), can be reproduced in two ways: (1) with coupling R4-I at *c* of 70.53 MHz and three other proton couplings of 95.96, 82.80, and 24.75 MHz; (2) with the measured value for R4-I, one proton coupling of 21.64 MHz, and one nitrogen coupling of 82.32 MHz (see Figures S10 and

TABLE 9: Hyperfine Coupling Tensors for Radical R4 (a) and the Comparisons between Tensor R4-I and α-Coupling Tensors from the C5-Dehydrogenation Radical from 298 K Irradiation Studied at 66 K (b) and at 298 K (c) in L-arg·HCl·H_2O Single Crystals Irradiated at 298 K[a–d]

(a)				eigenvectors[b]		
coupling	principal value[a,b]	isotropic value[a]	anisotropic value[a]	*a*	*b*	*c**
R4-I	−102.26(5)	−61.45	−40.81	0.736(0)	0.423(1)	−0.529(1)
	−52.72(4)		8.73	0.639(1)	−0.176(1)	0.749(0)
	−29.38(6)		32.07	−0.223(0)	0.889(1)	0.400(1)

(b)			eigenvector				
tensor	isotropic value[a]	anisotropic value[a]	*a*	*b*	*c**	tensor	ang diff (deg)[c]
1_L	−59.81	−30.81	0.686	0.408	−0.601	:R4-I	5.5
		−0.85	0.726	−0.389	0.567		16.9
		31.66	0.002	0.826	0.564		16.4

(c)			eigenvector				
tensor	isotropic value[a]	anisotropic value[a]	*a*	*b*	*c**	tensor	ang diff (deg)[c]
1_R	−56.76	−32.76	0.696	0.421	−0.582	:R4-I	3.4
		1.26	0.717	−0.355	0.600		14.1
		31.50	−0.046	0.835	0.549		13.5

[a] Values in MHz. [b] Numbers in parentheses are the estimated uncertainties in the respective values as reported by the statistical analysis. [c] Preliminary results from 298 K studies, not yet published. [d] "Angle diff (deg)" are the angular differences in degrees between the eigenvectors of tensor R4-I and those of tensors 1_L (66 K) and 1_R (298 K).

S11 of the Supporting Information). However, it is very unlikely that R4 is from the second set of couplings because the nitrogen coupling of 82.3 MHz is too large for any reasonable structure. For example, the nitrogen coupling in R3 is only ∼40 MHz, and the nitrogen couplings in R1a/R1b (the carboxyl radical anions) and in R2 (the decarboxylation radical) are smaller than 10 MHz. Also, if this large nitrogen coupling is due to the spin mainly located on a nitrogen atom, then it is inconsistent with the result that coupling R4-I is from a C−H α proton. On the basis of these points, we concluded that the main couplings of R4 are from four protons.

The EIE obtained by choosing ENDOR line R4-I for B//*c* from the partially deuterated crystal has the pattern of 1:2:2:1 (Figure 1 right) similar to that from the normal crystal (Figure 1 left), and its width is less than that from the normal crystal by ∼28 MHz. Moreover, the EIE pattern (B//*c*) from the partially deuterated crystal can be reproduced well by using only the couplings of 95.96, 82.80, and 70.53 MHz (see Figure S10 of the Supporting Information). These results indicate that the smallest coupling of 24.75 MHz in the simulated EIE for the normal crystal is from an exchangeable proton. From these characteristics, and the structure of the arginine molecule, R4 has two possible identities: the radical from dehydrogenation at C5 (see Chart 2), and the decarboxylation radical (see Chart 4). Both structures can exhibit one exchangeable and three nonexchangeable couplings, with one of the nonexchangeable couplings from an α-proton.

We concluded that R4 is the product of H-abstraction from C5 for two reasons. One is that couplings A-D of R2, which was identified above as the decarboxylation radical, are quite different from those of R4: the angular differences between the eigenvectors of α-coupling A listed in Table 4 and of R4-I are larger than 45°, the exchangeable β-couplings B and D are both larger than that of R4 by ∼40 MHz; the nonexchangeable β-coupling C is smaller than those in R4 by ∼30 MHz. The second reason is that preliminary analysis of stable radicals in crystals irradiated at room temperature indicates the presence of radicals with couplings similar to those in R4 under those conditions. Decarboxylation radicals typically are unstable at room temperature; it is also difficult to imagine that they would undergo the extensive geometric reorientation necessary to account for the β-couplings indicated by the EIE analysis.

Therefore, the above results support the identification that R4 is the result of dehydrogenation at C5. In this structure, the spin is mainly on C5, the α-coupling R4-I is from H9 (or H10), the nonexchangeable couplings are from H7 and H8, and the exchangeable coupling is from H11.

3.10. Radical R5: An Unidentified Product. EIE from R5 in the normal crystal was detected only for B//*a* (see Figure 8 S12 of the Supporting Information). The only ENDOR line observed for R5 was labeled as "R5-I." (The tensor from it, characteristic of a β-coupling, is listed in Table S3 of the Supporting Information.) Because line R5-I was very weak in the ENDOR (B//*a*) for the normal and the partially deuterated crystals, it is uncertain if coupling R5-I is from an exchangeable proton because it was not possible to obtain EIE from R5 in the partially deuterated crystals.

It is possible that R5 is still another conformation of the carboxyl-centered reduction radical (see Chart 3). If so, then R5-I can be ascribed to H4. However, the eigenvector* of R5-I is quite different from crystallographic direction H4···C1 in both molecules A and B, and tensor R5-I is quite different from tensors a1 and b1 described above. These points argue against the possibility that R5 is another version of the carboxyl-centered radical, but the available evidence is insufficient to identify it.

4. Summary and Discussion

In many respects L-arg·HCl·H_2O behaves like other amino acids upon exposure to ionizing radiation: one-electron oxidation leads to decarboxylation, and electron capture (one-electron reduction) leads to a product (the carboxyl "anion") with unpaired spin localized on the carboxyl group.[31] (In addition, preliminary analyses of results from warming the crystals to room temperature, and from irradiation at room temperature, indicate a significant contribution to the EPR from the deamination radical, a common product of the carboxyl anion.) Because the crystals contained two molecules with slightly different conformations of the carboxyl moiety, there were two forms of the carboxyl-centered radical (R1a and R1b). In both

cases, computational modeling supported the identifications and indicated movement of neighboring hydrogen-bonded protons toward the carboxyl oxygens.

Detection of a second product of one-electron reduction, in which the unpaired electron was localized on the guanidyl of the arginine side chain (R3), is more unusual. Identification of this product was supported by computational modeling and spectrum simulations. However, the obvious question is why this system should lead to two so apparently distinct initial products of one-electron reduction. The cluster model calculations offer a clue to this. Specifically, a full arginine model was used in the cluster models of both reduction products. However, for the carboxyl-centered product, the cluster focused on the hydrogen bonding environment of the carboxyl but selectively froze the coordinates of several atoms (including those of the amino and guanidyl moieties) to model the constraints on reconformation imposed by the crystal environment. A similar approach was taken for the guanidyl-centered product as shown in Figure 5. In both cases, the computational results showed the unpaired electron localized on the moiety engaged in hydrogen bonding. Thus the results do not address the question of how the electron initially attached to the two groups: perhaps they are approximately equally attractive for an electron and one attaches simply on the basis of the random probability that it is closer to one or the other group. However, the modeling calculations make it clear that the hydrogen bonding environment is important to stabilizing the products in each case.

The consequences of electron attachment to peptides, and the description of their mechanistic details, have been a recent topic of interest in the mass spectroscopy community; a particular focus has been the role of electron attachment in leading to selective cleavage of the N−C_α bond of the peptide backbone.[32] For individual amino acids this reaction leads to deamination and its connection to the carboxyl anion in condensed media is well-known.[31] Because the "carboxyl anion" can be stabilized at sufficiently low temperatures, it is clear that there is an activation barrier to the deamination reaction in the condensed phase. One question important to understanding the mechanism of N−C_α cleavage in condensed systems is if the reaction is inter- or intramolecular. Most assume that it is an intramolecular event and work by Shields and Hamrick[33] gave evidence supporting this view: they found that the reaction's "activation temperature" could be correlated with the angle between the N−C_α bond and the orbital of the unpaired electron. Their results can be interpreted as indicating that this angle controls thermal activation (e.g., vibration) of electron transfer from the carboxyl to the amino group, and thus that it controls the intramolecular process of deamination, i.e., N−C_α bond cleavage. Earlier work by Sevilla,[34] and by Sinclair and Codella,[35] found evidence from simple peptides that the electron, initially trapped on the C-terminal carboxyl group, migrated along the peptide chain to a more general peptide linkage with the end result being N−C_α cleavage. In their computation-based investigation of molecules in the gas phase, Syrstad and Tureček[32] extend to the N−C_α cleavage process the idea initiated by Sawicka et al.,[36] that local charge centers exert a significant influence on this process. Because amino acids typically crystallize as zwitterions, and often as protonated cations from acidic solutions (e.g., L-arg·HCl·H_2O), local charge centers are prevalent in these condensed systems. Therefore, results from the solid and gas phases are mutually supportive and complementary. (In fact, for modeling studies, crystal systems have the significant benefit that the initial molecular associations are well-defined and well-known via diffraction analyses.)

Previous work on protein−DNA systems, in which direct ionization of the two components led to the end products, found clear evidence that electrons migrate from protein to DNA while the electron-loss centers remain within the respective components.[5,37] On that basis, electron trapping by the protein backbone is unlikely to have a major consequence for DNA. As well, the decarboxylation product observed here (R2) is unlikely to indicate a reaction of major consequence for chromatin because an intact carboxyl group is present only at the C-terminus of a protein. (We note, however, the evidence for radiation damage leading to the loss of carboxyl group definition in the diffraction analysis of a protein.[38]) Oxidation also leads to products with spin localized on the amino acid side chain such as the C5-centered H-abstraction radical reported here. Experimental challenges have meant that relatively few reports have appeared that describe the individual nucleobases and amino acids involved in DNA−protein cross-links (DPCs).[39] Mainly, those appearing have consisted of lysine-guanine linkages investigated as a consequence of DNA oxidation.[40] However, the potential that oxidation products of proteins can attack DNA leads to a focus on those amino acid side chains most commonly in contact with DNA, and arginine is the most common of these. Thus, a product such as R4 reported here is in position to form a covalent bond to DNA within chromatin,[41] and in other instances in which proteins and DNA interact. As well, radical R3 in the gas phase was found to abstract a hydrogen from other sites within the peptide.[42] With its close proximity to DNA in chromatin, such a radical also might abstract hydrogen from the DNA bases if it is competitive with DNA for ionization-produced electrons.

Supporting Information Available: Tables S1 and S2 showing hyperfine couplings computed for R2 from molecule B and for R3 from molecule B. Table S3 shows the hyperfine tensor measured for R5. Figures S1−S4, S6, S9, and S13 show the angular dependence of experimental data from all radicals. Figures S5, S7, and S10−S12 compare experimental spectra to those simulated with the measured tensors. Figure S8 with its associated text shows and describes the ENDOR evidence for the nitrogen coupling of R3. This material is available free of charge via the Internet at http://pubs.acs.org.

References and Notes

(1) Wolffe, A. *Chromatin: Structure and Function*; Academic Press: San Diego, 1998.

(2) Davey, C. A.; Sargent, D. F.; Luger, K.; Maeder, A. W.; Richmond, T. J. *J. Mol. Biol.* **2002**, *319*, 1097.

(3) Luscombe, N. M.; Laskowski, R. A.; Thornton, J. M. *Nucleic Acids Res.* **2001**, *29*, 2860.

(4) (a) Cullis, P. M.; Jones, G. D. D.; Symons, M. C. R.; Lea, J. S. *Nature (London)* **1987**, *330*, 773. (b) Lloyd, P. H.; Peacocke, A. R. *Proc. R. Soc. (London)* **1966**, *B164*, 40. (c) Mee, L. K.; Adelstein, S. J. *Radiat. Environ. Biophys.* **1987**, *26*, 13. (d) Ly, A.; Tran, N. Q.; Sullivan, K.; Bandong, S. L.; Milligan, J. R. *Org. Biomol. Chem.* **2005**, *3*, 917. (e) Newton, G. L.; Ly, A.; Tran, N. Q.; Ward, J. F.; Milligan, J. R. *Int. J. Radiat. Biol.* **2004**, *80*, 643. (f) Milligan, J. R.; Aguilera, J. A.; Ly, A.; Tran, N. Q.; Hoang, O.; Ward, J. F. *Nucleic Acids Res.* **2003**, *31*, 6258.

(5) (a) Faucitano, A.; Buttafava, A.; Martinotti, F.; Pedraly-Noy, G. *Radiat. Phys. Chem.* **1992**, *40*, 357. (b) Weiland, B.; Hüttermann, J. *Int. J. Radiat. Biol.* **2000**, *76*, 1075.

(6) Zhou, Y.; Nelson, W. H. *Radiat. Phys. Chem.* **2010**, *79*, 479.

(7) Joshi, A.; Johnsen, R. H. *J. Phys. Chem.* **1976**, *80*, 46.

(8) Aydin, M.; Başkan, M. ; Yakar, S.; Ulak, F. ; Aydinol, M.; Aydinol, B.; Büyüm, M. *Radiat. Eff. Defects Solids* **2008**, *163*, 41.

(9) Olsen, B., Strålingsinduserte radikaler i enkrystaller av L-arginin monofosfat monohydrat ved 295 K og 77 K. Master's Thesis, University of Oslo, 2008.

(10) (a) Chen, X.; Tureček, F. *J. Am. Chem. Soc.* **2006**, *128*, 12520. (b) Panja, S.; Nielsen, S. B.; Hvelplund, P.; Tureček, F. *J. Am. Soc. Mass Spectrom.* **2008**, *19*, 1726.

(11) Dow, J.; Jensen, L. H.; Mazumdar, S. K.; Srinivasan, R.; Ramachandran, G. N. *Acta Crystallogr.* **1970**, *B26*, 1662.

(12) Nelson, W. H.; Hole, E. O.; Sagstuen, E.; Close, D. M. *Int. J. Radiat. Biol.* **1988**, *54*, 963.

(13) (a) Duling, D. R.; Motten, A. G.; Mason, R. P. *J. Magn. Reson.* **1988**, *77*, 504. (b) Duling, D. R. *J. Magn. Reson.* **1994**, *B104*, 105.

(14) Frisch, M. J.; Trucks, G. W.; Schlegel, H. B.; Scuseria, G. E.; Robb, M. A.; Cheeseman, J. R.; Montgomery, J. A., Jr.; Vreven, T.; Kudin, K. N.; Burant, J. C.; Millam, J. M.; Iyengar, S. S.; Tomasi, J.; Barone, V.; Mennucci, B.; Cossi, M.; Scalmani, G.; Rega, N.; Petersson, G. A.; Nakatsuji, H.; Hada, M.; Ehara, M.; Toyota, K.; Fukuda, R.; Hasegawa, J.; Ishida, M.; Nakajima, T.; Honda, Y.; Kitao, O.; Nakai, H.; Klene, M.; Li, X.; Knox, J. E.; Hratchian, H. P.; Cross, J. B.; Adamo, C.; Jaramillo, J.; Gomperts, R.; Stratmann, R. E.; Yazyev, O.; Austin, A. J.; Cammi, R.; Pomelli, C.; Ochterski, J. W.; Ayala, P. Y.; Morokuma, K.; Voth, G. A.; Salvador, P.; Dannenberg, J. J.; Zakrzewski, V. G.; Dapprich, S.; Daniels, A. D.; Strain, M. C.; Farkas, O.; Malick, D. K.; Rabuck, A. D.; Raghavachari, K.; Foresman, J. B.; Ortiz, J. V.; Cui, Q.; Baboul, A. G.; Clifford, S.; Cioslowski, J.; Stefanov, B. B.; Liu, G.; Liashenko, A.; Piskorz, P.; Komaromi, I.; Martin, R. L.; Fox, D. J.; Keith, T.; Al-Laham, M. A.; Peng, C. Y.; Nanayakkara, A.; Challacombe, M.; Gill, P. M. W.; Johnson, B.; Chen, W.; Wong, M. W.; Gonzalez, C.; Pople, J. A. *Gaussian 03*; Rev. B.04; Gaussian Inc.: Pittsburgh, PA, 2003.

(15) Becke, A. D. *J. Chem. Phys.* **1996**, *104*, 1040.

(16) Vanhaelewyn, G. C. A. M.; Jansen, B.; Pauwels, E.; Sagstuen, E.; Waroquier, M.; Callens, F. J. *J. Phys. Chem. A* **2004**, *108*, 3308.

(17) Pauwels, E.; Van Speybroeck, V.; Waroquier, M. *J. Phys. Chem. A* **2004**, *108*, 11321.

(18) Muto, H.; Iwasaki, M. *J. Chem. Phys.* **1973**, *59*, 4821.

(19) (a) Muto, H.; Nunome, K.; Iwasaki, M. *J. Chem. Phys.* **1974**, *61*, 1075. (b) Muto, H.; Nunome, K.; Iwasaki, M. *J. Chem. Phys.* **1974**, *61*, 5311. (c) Iwasaki, M.; Muto, H. *J. Chem. Phys.* **1974**, *61*, 5315.

(20) In the text, "eigenvector*" denotes the vector associated with the maximum eigenvalue for β-couplings.

(21) Heller, C.; McConnell, H. M. *J. Chem. Phys.* **1960**, *32*, 1535.

(22) Muto, H. Trapped anions in organic crystals. In *Radical Ionic Systems*; Kluwer: Amsterdam, 1991; pp 337−359.

(23) Øhman, K. T.; Sanderud, A.; Hole, E. O.; Sagstuen, E. *J. Phys. Chem. A* **2006**, *110*, 9585.

(24) McConnell, H. M.; Chesnut, D. B. *J. Chem. Phys.* **1958**, *28*, 107.

(25) Bernhard, W. A. *J. Chem. Phys.* **1984**, *81*, 5928.

(26) Gordy, W. *Theory and Applications of Electron Spin Resonance*; Wiley: New York, 1980.

(27) Fessenden, R. W.; Schuler, R. H. *J. Chem. Phys.* **1963**, *39*, 2147.

(28) Erling, P. A.; Nelson, W. H. *J. Phys. Chem. A* **2004**, *108*, 7591.

(29) Tomasi, J.; Mennucci, B.; Cammi, R. *Chem. Rev.* **2005**, *105*, 2999.

(30) Zhou. Y.; Nelson, W. H. Unpublished work.

(31) Sagstuen, E.; Sanderud, A.; Hole, E. O. *Radiat. Res.* **2004**, *162*, 112.

(32) Syrstad, E. A.; Tureček, F. *J. Am. Soc. Mass Spectrom.* **2005**, *16*, 208.

(33) Shields, H.; Hamrick, J.; Phillip, J. *J. Chem. Phys.* **1976**, *64*, 263.

(34) Sevilla, M. D. *J. Phys. Chem.* **1970**, *74*, 3366.

(35) Sinclair, J.; Codella, P. *J. Chem. Phys.* **1973**, *59*, 1569.

(36) Sawicka, A.; Skurski, P.; Hudgins, R. R.; Simons, J. *J. Phys. Chem. B* **2003**, *107*, 13505.

(37) Symons, M. C. R. *Free Radicals Biol. Med.* **1997**, *22*, 1271.

(38) Fioravanti, E.; Vellieux, F. M. D.; Amara, P.; Madern, D.; Weik, M. *J. Synchrotron Rad.* **2007**, *14*, 84.

(39) Barker, S.; Weinfeld, M.; Murray, D. *Mutat. Res.* **2005**, *589*, 111.

(40) (a) Morin, B.; Cadet, J. *J. Am. Chem. Soc.* **1995**, *117*, 12408. (b) Perrier, S.; Hau, J.; Gasparutto, D.; Cadet, J.; Favier, A.; Ravanat, J.-L. *J. Am. Chem. Soc.* **2006**, *128*, 5703. (c) Johansen, M. E.; Muller, J. G.; Xu, X.; Burrows, C. J. *Biochemistry* **2005**, *44*, 5660. (d) Xu, X.; Muller, J. G.; Ye, Y.; Burrows, C. J. *J. Am. Chem. Soc.* **2008**, *130*, 703.

(41) Bjorklund, C. C.; Davis, W. B. *Biochemistry* **2007**, *46*, 10745.

(42) Hayakawa, S.; Matsubara, H.; Panja, S.; Hvelplund, P.; Nielsen, S. B.; Chen, X.; Tureček, F. *J. Am. Chem. Soc.* **2008**, *130*, 7645.

JP911943N